JOURNAL OF THERMOPHYSICS AND HEAT TRANSFER
Vol. 20, No. 2, April–June 2006

Local Heat/Mass Transfer Phenomena in Rotating Passage, Part 2: Angled Ribbed Passage

Kyung Min Kim,* Yun Young Kim,† Dong Hyun Lee,‡ Dong Ho Rhee,§ and Hyung Hee Cho¶
Yonsei University, Seoul 120-749, Republic of Korea

Mass transfer experiments and numerical computations are conducted to investigate the heat/mass transfer and flow characteristics in a rotating passage with a 180-deg turn. In the present study, rectangular 70-deg rib turbulators are attached in cross and parallel arrangements on the leading and trailing surfaces of the passage. The cross-sectional area of the passage is 20 × 40 mm^2, and the pitch-to-rib height ratio (p/e) is 7.5. The rotation number ranges from 0.0 to 0.20, whereas the Reynolds number is constant at 10,000. The results reveal that the angled rib turbulators enhance significantly heat/mass transfer in the rotating two-pass duct by generating a secondary flow. For the cross-ribbed passage, a heat/mass transfer discrepancy is observed in the second pass even for the stationary case because one asymmetric cell of secondary flow is induced in the first pass and turning region. For the parallel-ribbed passage, the flow and heat/mass transfer characteristics are less subject to the rotation number than those of the former case due to the different flow structure. At the highest tested rotation number ($Ro = 0.20$), the turn-induced single vortex cell becomes identical regardless of the rib configuration so that the local heat/mass transfer distributions are similar in the turning region for all of the test sections.

Nomenclature

D_h = hydraulic diameter, m
D_{naph} = mass diffusion coefficient of naphthalene vapor in air, $\text{m}^2 \cdot \text{s}^{-1}$
e = rib height, m
H = passage height, m
h = heat transfer coefficient, $\text{W} \cdot \text{m}^{-2} \cdot \text{K}^{-1}$
h_m = mass transfer coefficient, $\text{m} \cdot \text{s}^{-1}$
k = thermal conductivity of coolant, $\text{W} \cdot \text{m}^{-1} \cdot \text{K}^{-1}$
p = rib-to-rib pitch, m
Re = Reynolds number, $D_h V/\nu$
Ro = Rotation number, $D_h \Omega / V$
Sc = Schmidt number, ν / D_{naph}
Sh = Sherwood number, $h_m D_h / D_{\text{naph}}$
Sh_0 = Sherwood number of a fully developed turbulent flow in a stationary smooth pipe, Eq. (2)
$\overline{Sh}$ = regional averaged Sherwood number,

$$\int_{x_1}^{x_1+p} \int_{y_1}^{y_2} Sh \, \mathrm{d}y \, \mathrm{d}x \Big/ \int_{x_1}^{x_1+p} \int_{y_1}^{y_2} \mathrm{d}y \, \mathrm{d}x$$

W = passage width, m
x = coordinate and distance in the streamwise direction, m
y = coordinate and distance in the lateral direction, m
z = coordinate and distance in the vertical direction, m
α = rib angle of attack
μ = dynamic viscosity, $\text{kg} \cdot \text{m}^{-1} \cdot \text{s}^{-1}$
ν = kinematic viscosity, $\text{m}^2 \cdot \text{s}^{-1}$
Ω = angular velocity, $\text{rad} \cdot \text{s}^{-1}$

Received 3 December 2004; revision received 29 April 2005; accepted for publication 2 May 2005.

*Graduate Student, School of Mechanical Engineering.
†Graduate Student, School of Mechanical Engineering.
‡Graduate Student, School of Mechanical Engineering.
§Research Associate, School of Mechanical Engineering.
¶Professor, School of Mechanical Engineering; hhcho@yonsei.ac.kr.

Introduction

HEAT transfer and fluid flow in rib-roughened internal cooling passages of gas turbine blades have been widely investigated over the years to produce turbine engines with better performance. With the understanding that heat transfer is enhanced greatly by installing rib turbulators that break boundary layers, disturb main flow, and promote convection, many researchers have concentrated on the effect of rib geometries on heat transfer in coolant passages. In this context, mainly design parameters such as rib height e, rib angle of attack α, rib-to-rib pitch p, cross-sectional shape, and rib arrangement have been studied.[1,2]

Heat transfer and flow characteristics in stationary channels with rib turbulators have been widely reported. In experimental studies, Olsson and Sunden[2] measured flow structures, heat transfer coefficients, and pressure drop characteristics in a channel with five rib configurations. They provided specific information on secondary flow patterns through laser Doppler velocimetry measurements and smoke wire visualization. In addition, the performance of rib turbulators was assessed from the obtained heat transfer and pressure drop results. Chen et al.[3] also conducted mass transfer experiments with a ribbed two-pass duct. They examined detailed heat/mass transfer distributions on four walls of a square duct with 90-deg rib turbulators, stating that high heat/mass transfer rates are observed near the rib ends and near the corners downstream of each rib. In numerical investigations, Iacovides and Raisee[4] studied convective heat transfer in a coolant passage with a U-bend. In their study, local Nusselt number distributions and flowfields in the interrib regions were examined with in-line and staggered rib configurations. Miyake et al.[5] performed direct numerical simulation in a 90-deg ribbed channel. They presented two direct numerical simulations: one of a sand-grain roughness wall flow and the other of flow having k-type roughness of periodically arranged ribs. Ooi et al.[6] simulated turbulent flows and heat transfer near the ribbed surface using $\nu^2 - f$, Spalart–Allmaras, and two-layer κ–ε turbulence models. It was found that heat transfer predictions by the $\nu^2 - f$ model were the most silmilar to the experimental values, whereas all other turbulence models produce a similar flow pattern.

The studies have extended further to angled rib turbulators.[1,7,8] Through a series of experimental and numerical investigations, it is reported that angled ribs produce secondary flow in the cooling passage, promoting heat transfer on the surfaces where the coolant flow impinges by the mixture of cold and hot fluids. The degree of heat transfer augmentation depends on the rib angle, and friction factors

also change accordingly. The studies have reported that 60 ~ 75 deg angled ribs provide the best heat transfer performance.

Heat transfer and flow characteristics in a ribbed passage become more complex when the passage rotates because the effect of Coriolis force appears. Taslim et al.[9] and Al-Qahtani et al.[10] studied heat transfer in a 45-deg rib-roughened one-pass duct with rotation. Their experimental and numerical data show that not only the rib turbulators but also duct rotation influences flow and heat transfer. Although rib turbulators enhance heat transfer, the rotation effect causes higher heat transfer on the trailing surface than on the leading surface in the case of radially outward flow. Some researchers employed coolant passages that contain 180-deg bends in their studies. Park et al.[11,12] conducted mass transfer experiments with a two-pass rotating channel. The effects of transverse ribs, Coriolis force, channel orientation, and a sharp turn were investigated. Local Sherwood number distributions were affected significantly with each experimental condition. Accordingly, the distributions on each surface (leading and trailing surfaces) became locally different. Lin et al.[13] performed a numerical study of flow and heat transfer in rotating ducts. Their results showed that the phenomena are extremely complicated with the presence of rib turbulators, turning region, and duct rotation due to the interactions of secondary flows. The symmetry of counter-rotating secondary flow induced by angled rib turbulators or a U-bend was distorted by the rotation, changing heat transfer patterns on the inside surfaces of duct. The investigations are expanded over the effects of advanced rib turbulators such as staggered half V-ribs (Hwang et al.[14]), V-shaped and angled ribs with gaps (Lee et al.[15]), and detached 90-deg ribs (Liou et al.[16]).

Most experiments have been conducted for measurements of averaged heat transfer in rotating channels. However, information of the detailed heat transfer distributions is essential in the design of internal channels to reduce thermal stress and to prevent hot spots on turbine blades. For those reasons, it has been a major interest of study to understand local heat transfer and flow characteristics in a stationary one-pass channel (Cho et al.[17–20]) and a rotating two-pass channel (Cho et al.[21–23] and Kim et al.[24]) with ribs.

For the stationary channel, the effects of various rib turbulators such as 90-deg ribs, angled ribs (33, 45, 60, and 70 deg) and discrete ribs on the heat/mass transfer and flowfield have been studied both experimentally and numerically, describing how the secondary flow induced by the angled ribs and how the gap flow of discrete ribs promotes local heat/mass transfer on the channel walls. For the rotating channel, the effects of 90- and 70-deg rib turbulators were investigated in conjunction with the influence of rotation and duct aspect ratios. In one of those studies, the angled ribs in four types of cross arrangement are employed for the Reynolds number of 2×10^4 when the rotation number is 0.0 and 0.1. The results show that the rotating direction of the secondary flow induced by the rib turbulators in each arrangement dominantly determined heat/mass transfer characteristics in the channels.

The first part of the present study[25] examined the heat transfer and flow characteristics of smooth channels for various rotation numbers and compared them with other researchers' heat transfer data. In this paper, ribs having a 70-deg angle of attack α are used to investigate heat/mass transfer in the ribbed channel.[1,17] Because gas turbine blades rotate faster than experimental conditions, that is, the rotation number Ro of the gas turbine blades is between 0.2 and 0.3, investigations are extended to understand rotation effects in cross and parallel rib-roughened passages. Changes of heat/mass transfer augmentation resulting from the different rib arrangements and rotational speed are studied experimentally through the measurements of detailed local heat/mass transfer coefficients. The flowfields in the rotating passage are also predicted numerically to help an understanding of its heat/mass transfer phenomena.

Experimental Apparatus

A. Rotating Facility

The experimental apparatus and the operating conditions are the same as those in described in Ref. 25. The Reynolds number based on a hydraulic diameter is maintained at 1×10^4 constantly. The rotation numbers range from 0.0 to 0.20, and the maximum rotation number, $Ro = 0.20$, corresponds to 420 rpm approximately.

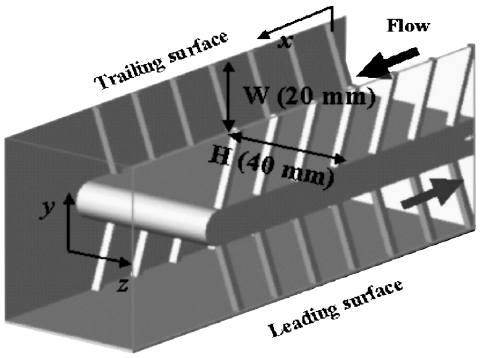

a) Cross rib arrangement

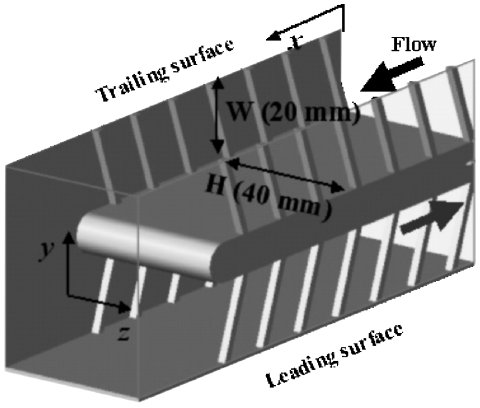

b) Parallel rib arrangement

Fig. 1 Geometry of the two-pass ribbed passage.

B. Test Section

Figure 1 is a three dimensional view of the test section. Overall dimensions are the same as those of the smooth passage used in Ref. 25. The difference is that 70-deg angled rib turbulators are attached on the inner walls (leading and trailing surfaces) in cross and parallel arrangements. The rib has a rectangular cross-sectional shape. The height e and width w are 2 mm and 3 mm, respectively. The pitch-to-rib height ratio (p/e) is 7.5, and the rib height-to-hydraulic diameter ratio (e/D_h) is 0.075. The coordinate system is presented in Fig. 2. The streamwise, lateral, and vertical directions correspond to the x, y, and z axis, respectively.

Experimental Procedure and Data Reduction

A naphthalene sublimation method is employed to obtain detailed heat/mass transfer coefficients on the passage walls. Detailed procedure and data reduction are the same as those in Ref. 25. From the local mass transfer coefficient h_m, the Sherwood number is calculated as

$$Sh = h_m D_h / D_{\text{naph}} \tag{1}$$

The uncertainty in the Sherwood number is estimated to be within ±7.7% at a 95% confidence level by using the uncertainty estimation method of Kline and McClintock.[26] The uncertainty of the naphthalene properties such as naphthalene vapor pressure with 6.4% error and diffusion coefficient with 3.1% error is most dominant in determining the uncertainty of the Sherwood number. The results are presented as the Sherwood number ratios, Sh/Sh_0, here. Sh_0 is the Sherwood number for a fully developed turbulent flow in a stationary smooth circular tube correlated by McAdams,[27]

$$Sh_0 = 0.023 Re^{0.8} Sc^{0.4} \tag{2}$$

Finally, The regional averaged Sherwood number $\overline{Sh}$ is calculated by the integration of the local Sherwood numbers weighted by

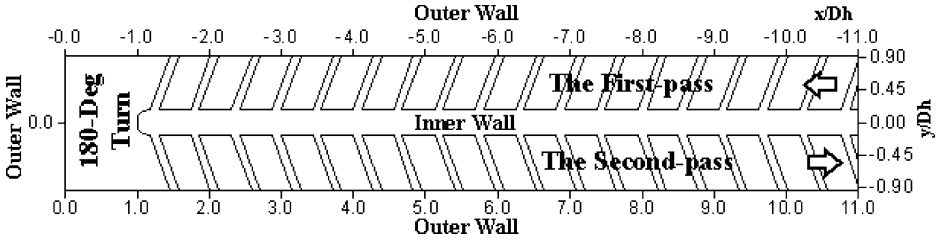

a) Cross ribs (leading)

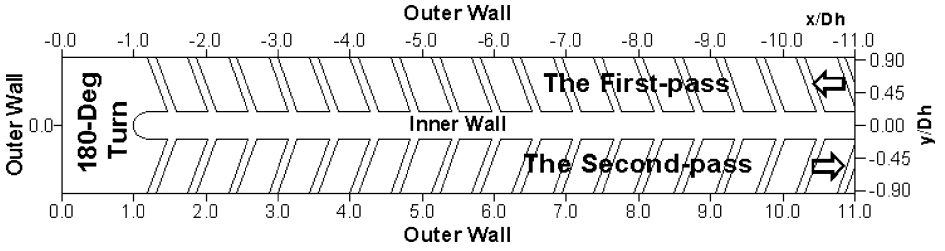

b) Cross ribs (trailing) and parallel ribs

Fig. 2 Coordinate system.

the pitch-to-pitch area. More detailed explanation is introduced in Ref. 25.

Numerical Conditions

Numerical simulations are performed using a commercial code (FLUENT 6.1) to understand the flow patterns in the stationary and rotating rib-roughened passage. The geometric and operating conditions are in accordance with those of the experimental study. The flowfields are analyzed using a re normalization group k–ε turbulent model with nonequilibrium wall function for the near-wall treatment, with an assumed three-dimensional incompressible and steady-state flow. The non equilibrium wall functions are suitable for use in complex flows involving separation, reattachment, and impingement, where the mean flow and turbulence are subjected to severe pressure gradients and change rapidly because of the capability to account partly for the effects of pressure gradients and departure from equilibrium.[28] Computational grids are created using the GAMBIT solid modeling. To simulate the flow patterns in the vicinity of ribbed surfaces with adequate resolution, 8 and 12 elements are evenly spread on the side and top surfaces of the angled rib turbulators, respectively, and the near-wall region was resolved to y^+ values ranging closest to 30 (Ref. 28). For all cases in the present part of investigation, the number of grid points is $44 \times 22 \times 744$ in each pass and $44 \times 64 \times 27$ in the turning region to obtain a grid-independent solution. The modeled geometry has a total of 1.5 milion grid points.

Results and Discussion

A. Internal Flow Phenomena

Figure 3 shows a schematic of secondary flow-inducing factors in the rotating cross and parallel ribbed passages with 180-deg turn. It is deduced from the present and previous results and is also a conventional way to display the internal flow patterns. The rectangle represents a cross-sectional view of the test section. Whereas only two factors, counter-rotating vortices induced by the 180-deg turn and the deflected flow by the rotation of passage, are found in the smooth passage, one cell of rib-induced secondary flow is additionally formed in the passage with ribs in the cross and parallel arrangement. The secondary flow by rib turbulator is indicated with dashed lines in Fig. 3, and its rotating direction is determined by the rib angle of attack. Accordingly, the interactions of those three factors change the internal flow and heat/mass transfer characteristics. Figure 3 supports the explanation of flowfields and local Sherwood number distributions in the cross and parallel ribbed passage.

Cross Ribs Arrangement

Figure 4a shows the numerically calculated flowfields in the cross ribbed passage for the Reynolds number of 1×10^4 and the rotation number of 0.0. In the first pass, it is observed that one cell of secondary flow is produced skewing along the passage walls in the clockwise direction because of the rib arrangement. The flow promotes convection adjacent to the ribbed surfaces. The turning region significantly influences the coolant flow, as revealed at $y/D_h = 0.0$ and $x/D_h = 1.225$. At turn entry of the first pass, the main flow is deflected toward the leading surface due to the cross ribs arrangement, and then one strong vortex cell is generated near the trailing surface on the 90-deg plane of the turn ($y/D_h = 0.0$). In the smooth duct, centrifugal force is exerted on the main flow passing the 180-deg turn, showing a pair of symmetric vortices as shown in Ref. 25. The effect of the turn still determinates the flow and heat/mass transfer characteristics after the exit of the turn. As the vortex propagates in the second pass, its center moves to the middle of the passage because of the interaction between the turn-induced and rib-induced secondary flows. Toward the downstream region, the vortex of the main flow becomes weaker due to the viscous dissipation and then mixes with the rib-induced secondary flow.

The calculated flow structure in the cross ribbed passage at a relatively low rotation number, $Ro = 0.05$, is shown in Fig. 4b. When the passage rotates, the influence of Coriolis force changes the flowfields noticeably. In the first pass, the overall flow structure is similar to that of the stationary case (the dashed line of Fig. 3a), but the flow is strengthened in the vicinity of the outer wall because of the interaction between the rotation-induced and rib-induced secondary flows, each of which rotates in the same direction near the wall. To the contrary, the flow is not reinforced significantly adjacent to the inner wall because the two secondary flows rotate in the opposite direction, colliding and weakening each other. The flow structure changes most distinctively in the turning region ($y/D_h = 0.0$ and $x/D_h = 1.225$). Compared with Fig. 4a, it is shown that another vortex cell is formed in the leading surface side and the one close to the trailing surface side contracts because of the deflected main flow from the first pass. At $x/D_h = 1.225$, two vortex cells are generated and determine the flow behavior in the upstream part of the second pass. However, at the downstream region, the vortices dissipate and the secondary flow induced by the rib turbulators overwhelms the flowfield.

The effect of rotation becomes stronger at the highest tested rotation number of 0.2 (Fig. 4c). The flow near the outer wall is strengthened more in the first pass, and the vortex close to the leading surface also expands significantly in the turn. In the upstream region of the second pass ($x/D_h = 1.787$), only a single vortex cell exists

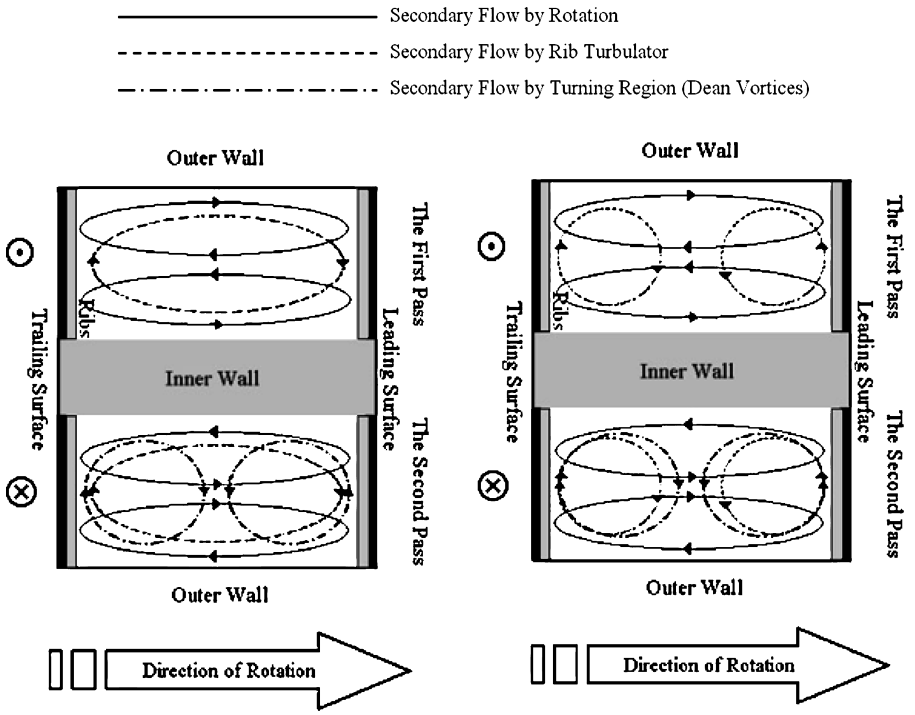

a) Cross-ribbed passage b) Parallel-ribbed passage

Fig. 3 Secondary flow-inducing factors: ——, by rotation; – – –, by rib turbulator; and – . – ., by turning region (Dean vortices).

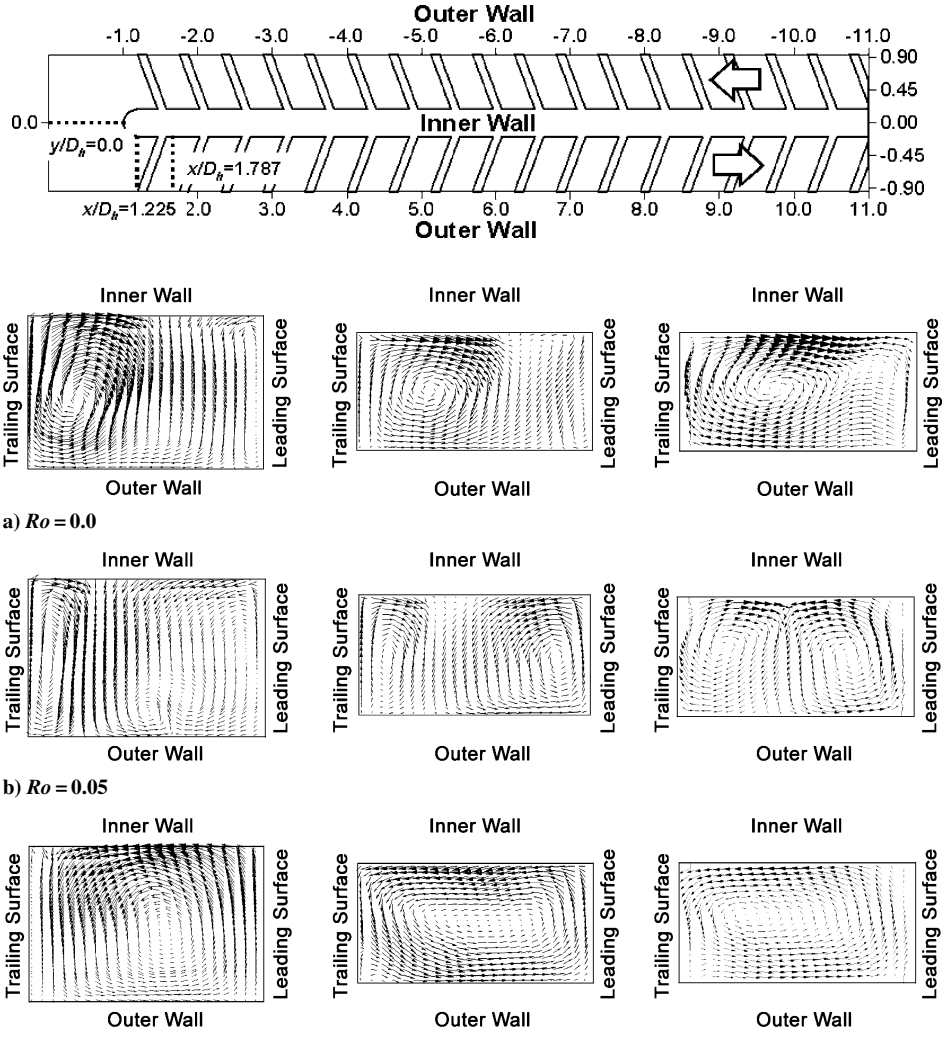

Fig. 4 Secondary flow patterns in the cross-ribbed passage, $Re = 1 \times 10^4$: left, $y/D_h = 0.0$; middle, $x/D_h = 1.225$; and right, $x/D_h = 1.787$.

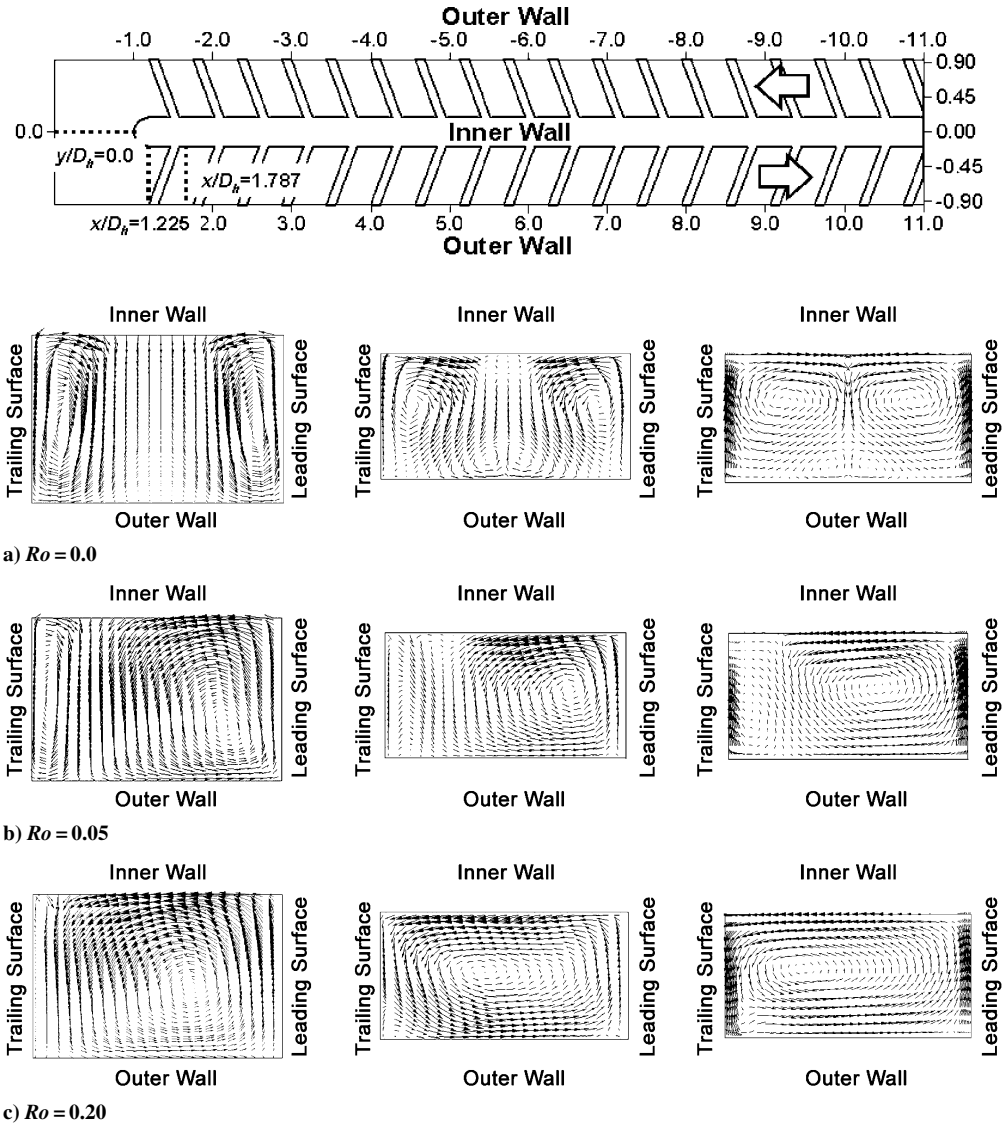

Fig. 5 Secondary flow patterns in the parallel-ribbed passage, $Re = 1 \times 10^4$: left, $y/D_h = 0.0$; middle, $x/D_h = 1.225$; and right, $x/D_h = 1.787$.

rotating in the counter-clockwise direction. The effect caused by the rotation of passage is so dominant that the rib-induced secondary flow is no longer observed at the rotation number of 0.20. As the flow reaches the outlet, the rotating direction of the secondary flow reverses with the diminishment of the turn-induced vortex. Notice that the resultant secondary flow adjoining the outer wall is strengthened because of the coinciding flow direction of the rib-induced and rotation-induced vortices.

Parallel Ribs Arrangement

Figure 5a shows the computational results of flowfields in the passage with the parallel rib arrangement for Reynolds number of 1×10^4 and rotation number of 0.0. Two rib-induced secondary flow cells are formed in the first pass. They impinge on the inner wall side of the leading and trailing surfaces and then move to the outer wall along the surfaces. In the middle of the turn ($y/D_h = 0.0$), turn-induced vortices are produced due to the centrifugal inertial force. The flow structure is similar to that of the smooth passage because the rib turbulators are symmetrically installed in the first pass. The influence of flow turning still remains in the upstream part of the second pass, and the secondary flow structure in the second pass is little changed because of the vortices induced by 180-deg turn and by the parallel ribs rotating in the same direction. However, the vortices wane in the downstream region because of the viscous dissipation.

The mixture of the three types of secondary flow, that is, the one by the Coriolis force, the rib turbulators, and the flow turning, creates a totally different flow structure in the rotating parallel ribbed passage (Figs. 5a and 5). In the first pass, the rib-induced secondary flow pushes the rotation-induced flow to the inner wall and strengthens the flow in the upper left corner of the passage (the schematic flow presented in Fig. 3). Therefore, the upper part of the rotation-induced secondary flow expands, and subsequently, the rib-induced secondary flow close to the leading surface shrinks. In the turning region, the earlier observed symmetric vortices on the 90-deg plane of the turn (Fig. 5a) no longer exist in the present case. Instead, the deflected main flow in the first pass enlarges the vortex cell close to the leading surface. The flow structure is still maintained in the upstream part of the second pass, showing a large vortex cell on the leading surface side and small one on the trailing surface side (Fig. 5b). As the flow proceeds, the flow pattern gradually transforms into one large vortex cell.

The effect of rotation is shown more significantly at the highest tested rotation number of 0.2 (Fig. 5c). In the turning region, the small vortex cell on the left side disappears and the one on the right side is aggrandized to the trailing surface because the main flow is more deflected at the rotation number of 0.20. Accordingly, only one cell of strong vortex is produced in the upstream of the second pass, and as it dissipates, a small vortex cell grows in the lower right corner of the passage. At the exit of the passage, the flow pattern changes into one pair of counter-rotating secondary flows that impinges to

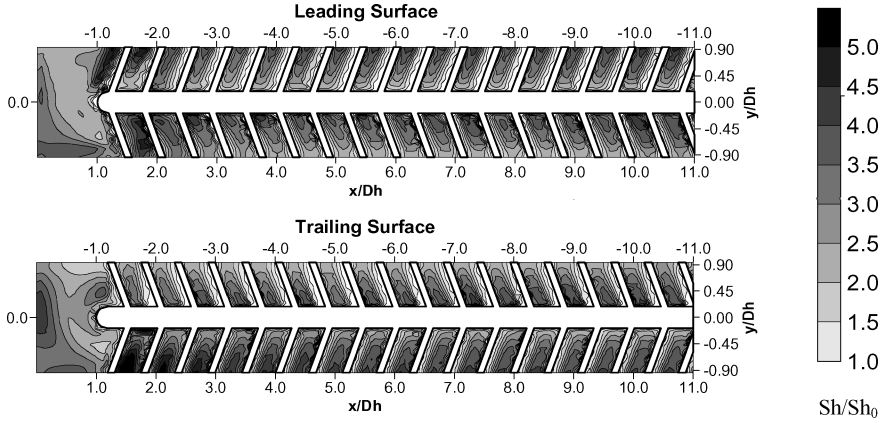

a) $Ro = 0.0$

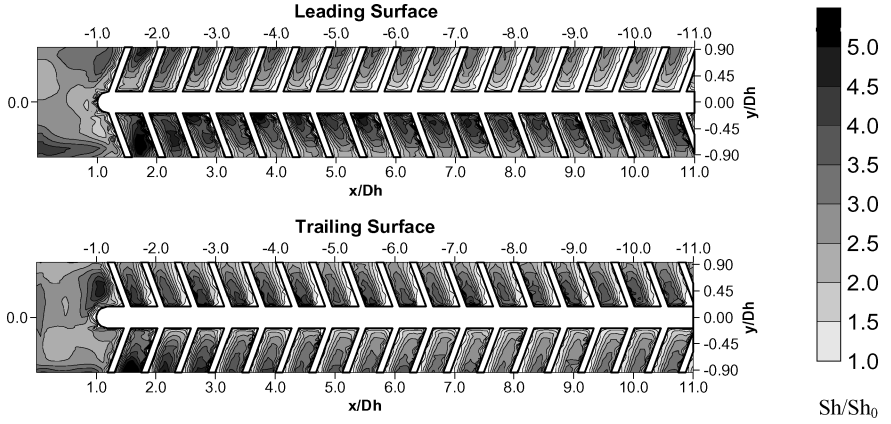

b) $Ro = 0.10$

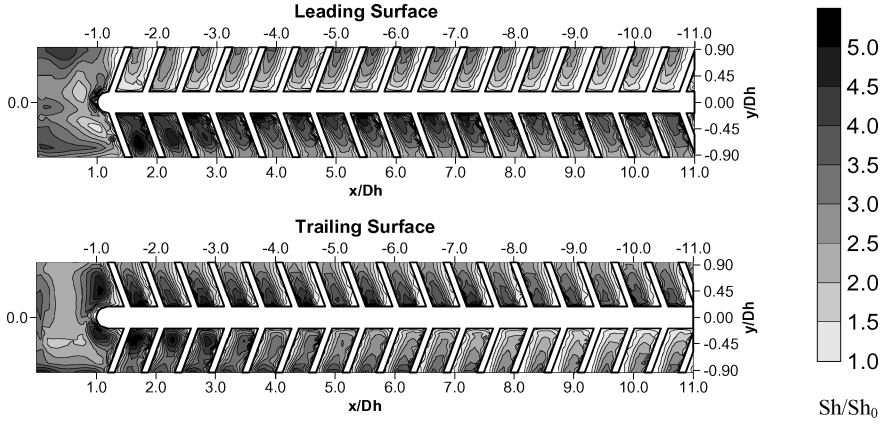

c) $Ro = 0.20$

Fig. 6 Local Sherwood number ratio distributions in the cross-ribbed passage.

the leading surface. The flow pattern is strikingly similar to that at the exit of the passage in the smooth duct.[25] The rotating direction of rib-induced secondary flow is the same as that of the Dean vortices in a second pass. The effect of rotation is the most dominant at the highest rotation number, the resultant flow behavior in the postturn region resembles those of the smooth passage at $Ro = 0.20$ (Ref. 25).

B. Local Heat/Mass Transfer Characteristics

Cross Rib Arrangement

Figure 6a shows the Sherwood number ratio distributions on the leading and trailing surfaces of the cross ribbed passage for the stationary case. High Sherwood number ratios are observed on the downward secondary flow sides, for example, the outer wall side of the leading surface ($y/D_h = 0.825$) and the inner wall side of the trailing surface ($y/D_h = 0.300$) in the first pass. This is consistent with the flow predictions presented in Fig. 4. In the turning region, heat/mass transfer is augmented on the 90- and 180-deg outer wall side of the turn because of the impingement of the vortex generated by the curvature of the turn. As numerically predicted in Fig. 4, the strong vortex is formed near the trailing surface so that heat/mass transfer augmentation is accordingly higher on the trailing surface. In the second pass, the effect of the 180-deg turn diminishes after approximately three to four rib pitches, and then heat/mass transfer patterns by the rib turbulators appear again on the passage walls. When it is considered that the turn-induced secondary flow dominates the heat/mass transfer to the middle of the second pass in the smooth passage,[25] its effect is curtailed in the ribbed duct because the rib-induced flow interferes with the propagation of the turn-induced vortex and finally mixes together.

With the rotation of passage, the heat/mass transfer characteristics become more complicated (Figs. 6b and 6c). In the first pass, the heat/mass transfer is enhanced on the trailing surface and

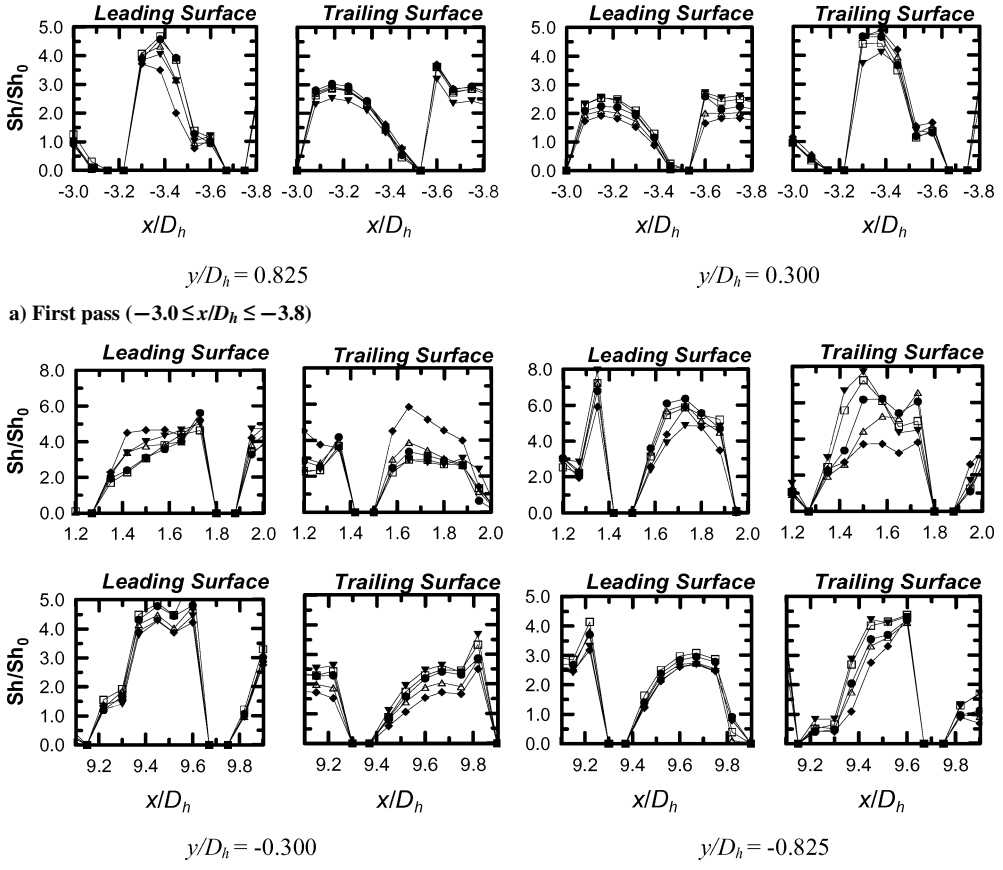

Fig. 7 Detailed Sh/Sh_0 distributions in the cross-ribbed passage: ▼, $Ro = 0.0$; □, $Ro = 0.5$; △, $Ro = 0.15$; and ♦, $Ro = 0.20$.

degenerated on the leading surface due to the deflection of the main flow by the Coriolis force. The discrepancy of heat/mass transfer enlarges with an increment of the rotation number. In the turning region, the high Sherwood number distribution at $x/D_h = -1.225$ disappears on the leading surface and expands on the trailing surface because the resultant vortex structure changes in the rotating ribbed duct. For example, the velocity vectors direct toward the trailing surface at the highest tested rotation number, $Ro = 0.20$. In the upstream region of the second pass, the heat/mass transfer characteristics on both leading and trailing surfaces are determined mainly by the effect of flow turning and rotation number. On the leading surface, the high Sherwood number ratios are locally observed near the outer wall side for all rotation numbers. However, on the trailing surface, the local region of heat/mass transfer augmentation initially located at $y/D_h = -0.90$ for the relatively low rotation number, $Ro = 0.05$, moves toward $y/D_h = -0.30$ as Ro increases. This location is consistent with the region where the turn-induced vortices impinge, as shown for $x/D_h = 1.787$ in Figs. 5b and 5c. In the downstream region, the vortices generated by the turning region become weaker, and thus, the heat/mass transfer discrepancy is observed again because the Coriolis force mainly determines heat/mass transfer characteristics. In this case, the main flow is deflected toward the leading surface due to the reversed direction of the Coriolis force. Therefore, the leading surface shows the higher Sherwood number ratios.

Specific local values of the Sherwood number ratios in a fully developed region of the first pass and the upstream and downstream regions of the second pass are presented in Fig. 7 to demonstrate the effect of rotation and flow turning on the heat/mass transfer augmentation. For the first pass (Fig. 7a), the distributions show the local heat/mass transfer in the lateral direction in one rib pitch: Sh/Sh_0 on the leading surface are affected greatly by the rotation more than those on the trailing surface. For the upstream region of the second pass ($1.2 \le x/D_h \le 2.0$ in Fig. 7b), as shown in Fig. 6, the heat/mass transfer is higher at $y/D_h = -0.825$, which is the measurement line nearby the outer wall, for a relatively low rotational speed, $Ro = 0.05$. As the passage rotates faster, $Ro = 0.15$, however, the difference of heat/mass transfer enhancement in the lateral direction becomes less significant, and then finally, at $Ro = 0.2$, the Sherwood number ratios are higher at the measurement lines nearby the inner wall, $y/D_h = -0.300$. Thus, Fig. 7 presents quantitatively the change of heat/mass transfer characteristics induced by flowfields in the rotating passage. For the downstream part of the second pass ($9.1 \le x/D_h \le 9.9$ in Fig. 7b), the rotational effect on heat transfer on the trailing surface is greater than that on the leading surface. The flow strength near the leading surface in the first pass (and the trailing surface in the second pass) is decreased because of the main flow deflected by the Coriolis force. In other words, it is the reason that reattachment of the secondary flow on the leading surface in the first pass by the cross-angled ribs becomes weaker than that of the other surface.

Figure 8 presents the regional averaged Sherwood number ratios taken from the earlier local distributions. In the first pass of the stationary duct, the cross rib arrangement enhances heat/mass transfer 2.5 times more than that of the nonribbed case overall. The Sherwood number ratios reach the peak value at $x/D_h = 1.254$ due to the effect of the turning region and then decrease as the flow proceeds. In the second pass, the heat/mass transfer discrepancy is observed, and the ratios are the higher on the trailing surface even though the passage does not rotate. This phenomenon is resulted from the asymmetric flow structure shown in Fig. 4. With the dissipation of the turn-induced single cell vortex, however, the Sherwood number ratios on the leading and trailing surfaces approach to each other at the outlet of the passage.

As the rotational speed increases, the difference of heat/mass transfer ratios between the leading and trailing surfaces increase. In the first pass, the heat/mass transfer is higher on the trailing surface, and in the second pass, it is higher on the leading surface. For instance, when Fig. 8a is compared with Fig. 8b, it is observed that the increment of the rotation number enlarges the heat/mass

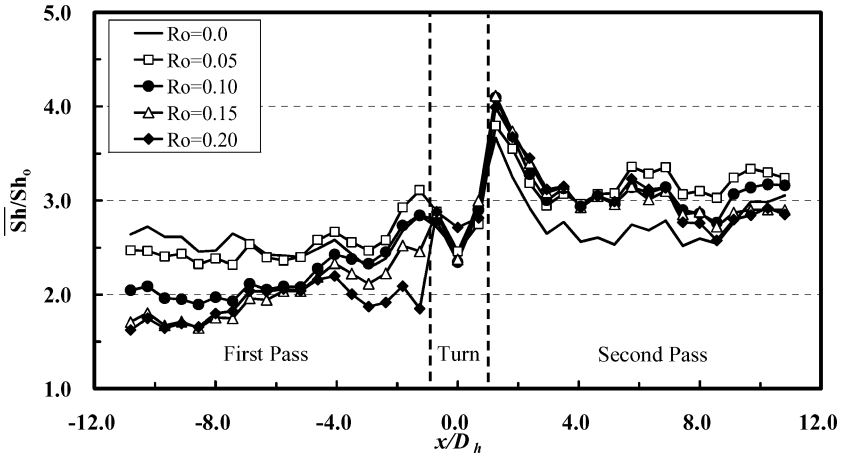

a) Leading surface

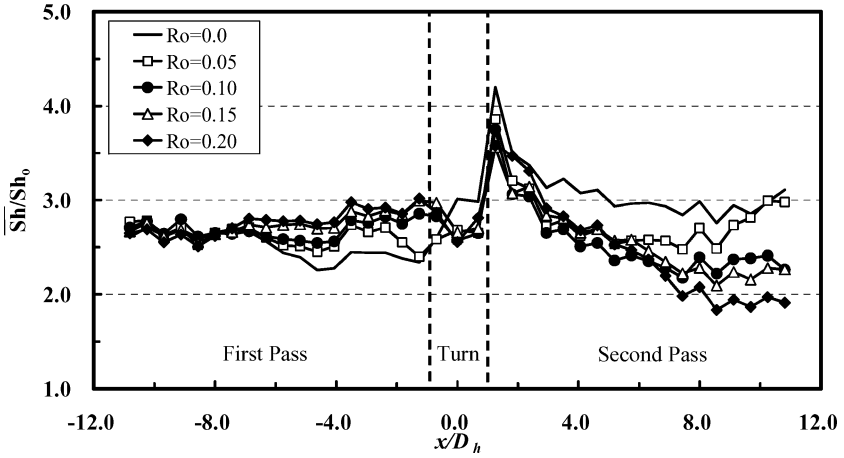

b) Trailing surface

Fig. 8 Regional averaged Sherwood number ratios in the cross-ribbed passage.

transfer discrepancy in downstream of the second pass. However, the higher rotation number produces lower Sherwood number ratios in the second pass on the same surface, for example, the trailing surface. This is because the vortex structure in the turn changes with the rotation number, as shown in Figs. 4b and 4c. In addition, as the rotation number increases, the influence of rotation becomes more dominant, overcoming the effect of the turn in the downstream region. The flow patterns presented in Figs. 4b and 4c support this behavior.

Parallel Rib Arrangement

Figure 9 presents the distributions of local Sherwood number ratios on the leading and trailing surfaces in the passage for the parallel rib arrangement. Figure 9a shows that both surfaces are practically the same for the stationary case. The heat/mass transfer is augmented in the regions where the rib-induced secondary flow impinges, as predicted in Fig. 5. At the entrance of the turn, an island of high heat/mass transfer region is observed on each surface, and the heat/mass transfer is also enhanced near the 90- and 180-deg outer wall of the turn. When compared with the results of the smooth passage, the area of heat/mass transfer augmentation is contracted because the resultant vortex cells in the turn are less vigorous in the present case. That is, the size and impingement regions of the vortices in the parallel rib channel are smaller and narrower than those of the smooth channel due to the difference of velocity profiles between the leading and trailing surfaces in the first pass. The local Sherwood number ratios are still high at the exit of the turn, $1.2 \le x/D_h \le 3.0$ and $y/D_h = -0.90$, but the effect of the 180-deg turn is weakened only after two to three rib pitches in the second pass.

When the passage channel rotates, the heat/mass transfer is augmented on the trailing surface and deteriorated on the leading surface in the first pass, as explained earlier. At the entrance of the 180-deg turn, $x/D_h = -1.225$, the high heat/mass transfer region on the leading surface, which is observed in the stationary passage (Fig. 9a), vanishes, whereas it still appears on the trailing surface. This is supported by the numerical simulation of the secondary flow at the location $x/D_h = 1.225$, in Fig. 5b. In the upstream part of the second pass, $1.2 \le x/D_h \le 3.0$, the heat/mass transfer is enhanced or sustained along the second pass. However, the vortices become weaker as the flow proceeds to the duct outlet, and therefore, the Coriolis force influences dominantly in the area of $6.0 \le x/D_h \le 11.0$ and the heat/mass transfer discrepancy between the trailing and leading walls is observed again.

At the highest tested rotation number of 0.2 (Fig. 9c), the rotation effect appears significant. On the leading surface, the heat/mass transfer pattern in the first pass is distorted so that the local augmentation on the inner wall side is not shown. When the corresponding flow patterns are considered, it is known that the secondary flow impinges mostly on the trailing surface and results in the high heat/mass transfer. Also note that the distorted distribution is observed as locally high heat transfer regions on the inner wall side in the first pass at $Ro = 0.10$, but as the passage rotates faster, the phenomena occur in the entire section of the first pass due to the strengthened Coriolis force. On the trailing surface, the high Sherwood number ratios are observed near the outer wall of the second pass, $1.2 \le x/D_h \le 4.0$ and $-0.93 \le y/D_h \le -0.45$, for the rotation number of 0.10, but it moves to the inner wall side with the increase of the rotational speed. The main reason is that the flow structure in the turning region changes from two counter-rotating vortices (Fig. 5b) to one cell of single vortex (Fig. 5c). The different location of the vortex impingement on the trailing surface influences the heat/mass transfer characteristic.

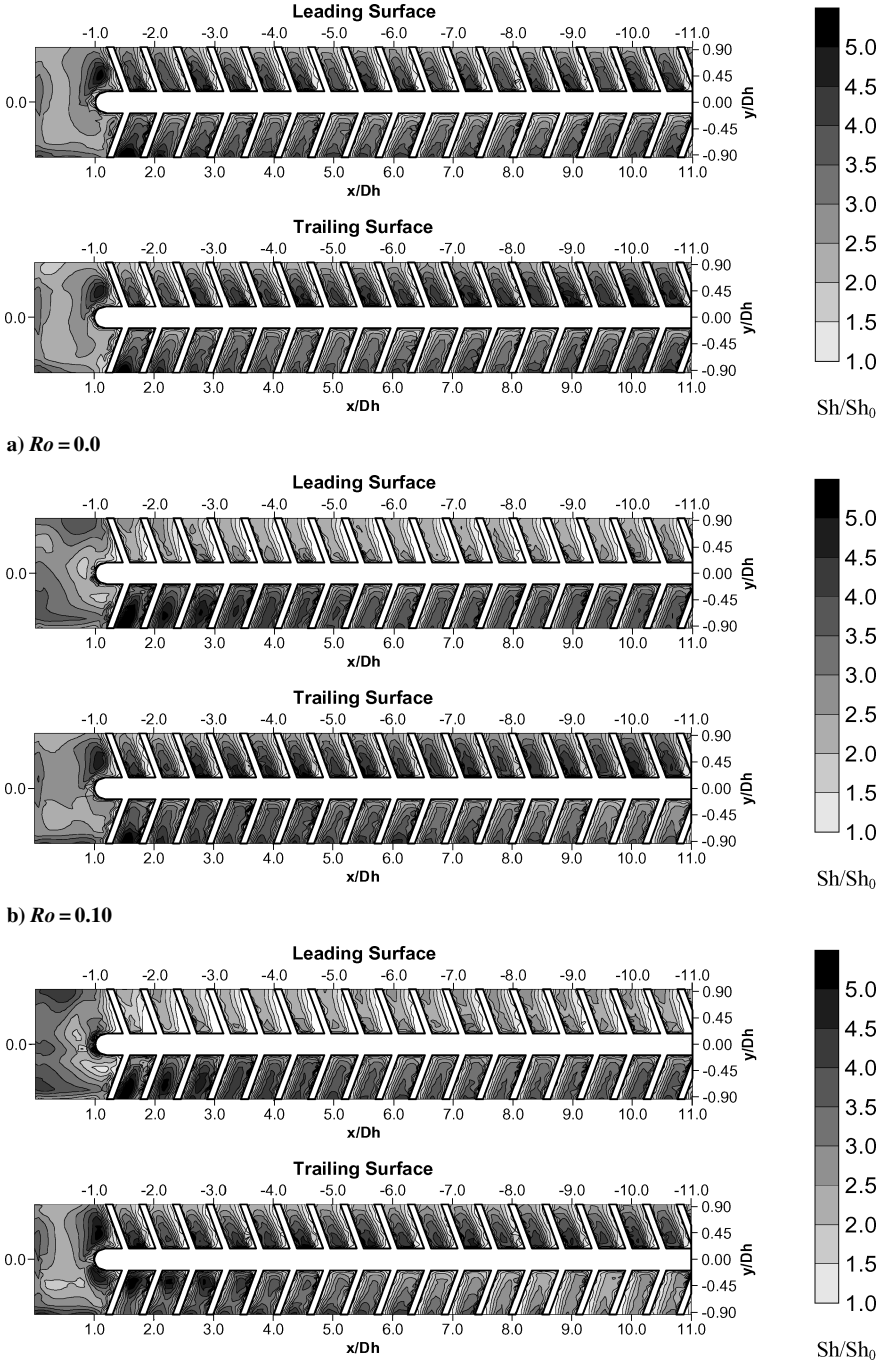

Fig. 9 Local Sherwood number ratio distributions in the parallel-ribbed passage.

The regional averaged Sherwood number ratios for the parallel rib arrangement are shown in Fig. 10. When the duct is roughened with rib turbulators, the average Sherwood number ratios in the stationary channel are approximately three times higher than those of the smooth passage.[25] In addition, Fig. 10 suggests that the impingement effect is even stronger in the parallel ribbed case than in the cross ribbed one. The Sherwood number ratios are slightly high at the passage inlet and approach to the fully developed value asymptotically in the first pass. The effect of the turning region is apparently shown right at $x/D_h = 1.254$ with the peak value of $\overline{Sh}/Sh_0$, and it soon disappears, leaving the effect of ribs again in the second pass. In the second pass, the peak Sherwood number ratios are shown at $x/D_h = 1.254$ and higher on the leading surface, which agrees with the internal flow phenomena, or the formation of large vortex cell close to the leading surface. The overall heat/mass transfer levels in the second pass are likely to be determined by the vortex structures after the turn, namely, the peak value at $x/D_h = 1.254$ is the highest in the entire second pass. The effect of the Coriolis force is observed after $x/D_h = 6.0$, deflecting the main flow toward the leading surface, so that the heat/mass transfer is higher on the leading surface at the same rotation number.

Detailed distributions of the local Sherwood number ratios in the upstream region of the second pass on the leading and trailing surfaces are selectively presented for all of the three channels (smooth, cross ribbed, and parallel ribbed channels) in Fig. 11. Note that $Sh/Sh_0 = 0$ indicates the positions of the ribs. For the stationary case (Fig. 11a), the resultant heat transfer distribution ranges in the turning region are distinctly different due to the rib arrangement. At the highest tested rotation number of 0.2, however, the effect of rotation dominates regardless of the rib arrangement on the trailing surface in the second pass. For instance, the specific values of local Sherwood numbers along the measurement lines are almost the

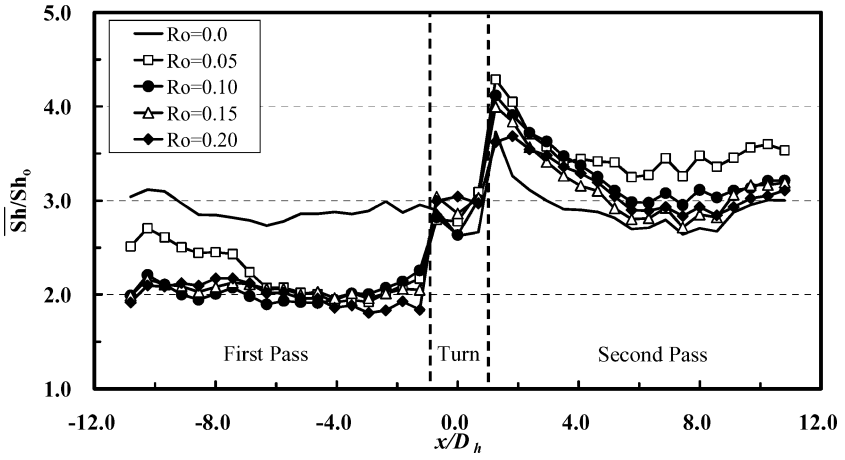

a) Leading surface

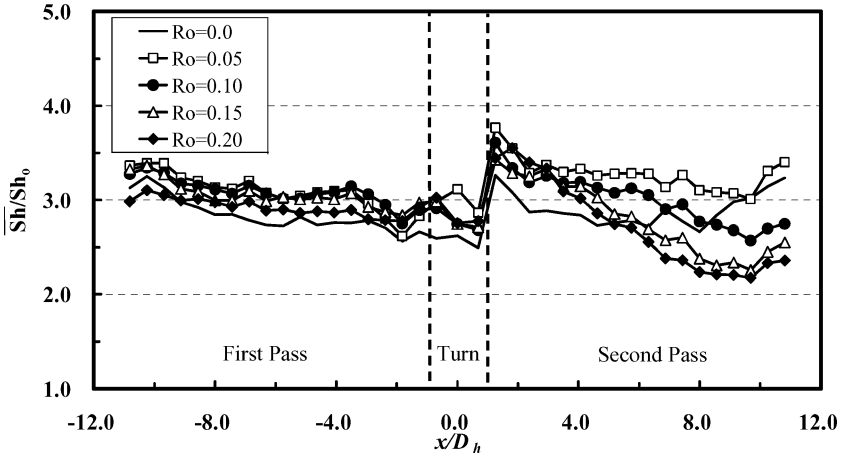

b) Trailing surface

Fig. 10 Regional averaged Sherwood number ratios in the parallel-ribbed passage.

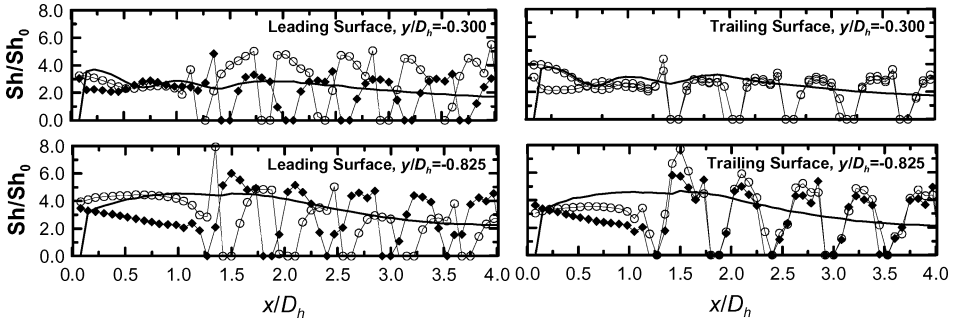

a) $Ro = 0.0$

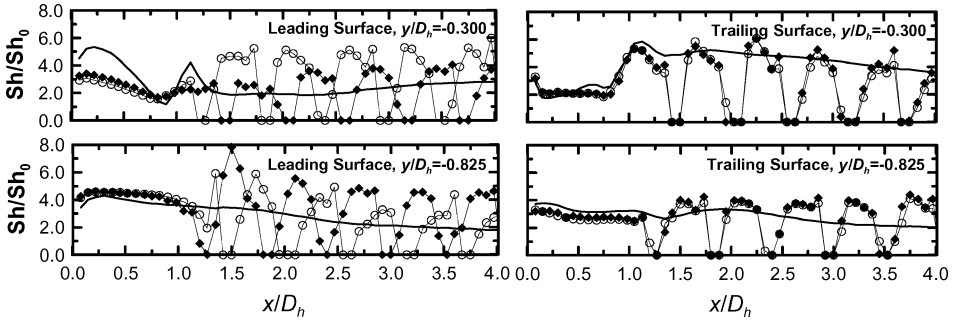

b) $Ro = 0.2$

Fig. 11 Detailed Sh/Sh_0 distributions in the second pass ($0.0 \le x/D_h \le 4.0$): ——, smooth; △, cross; and ♦, parallel.

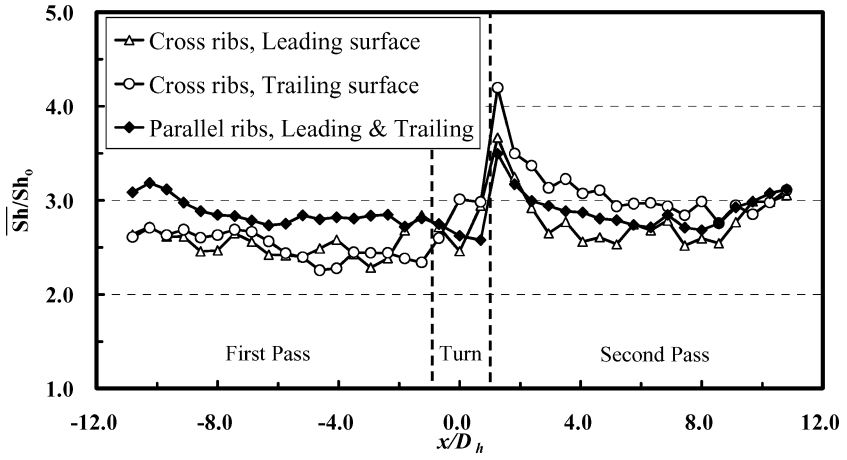

a) $Ro = 0.0$

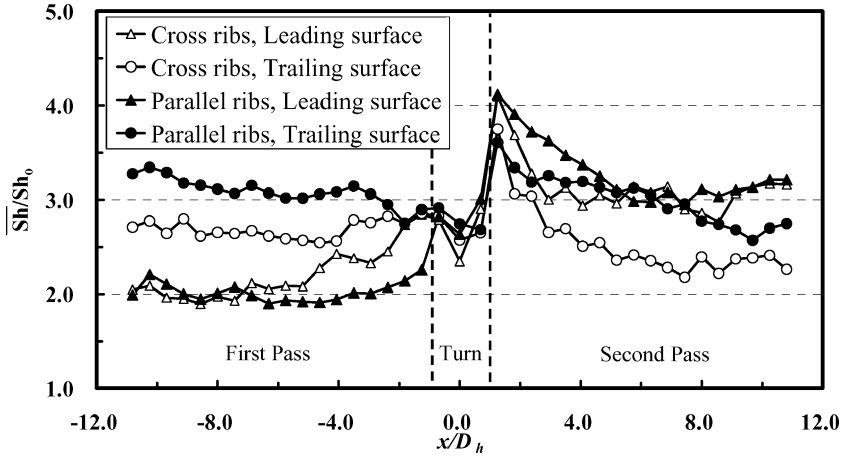

b) $Ro = 0.10$

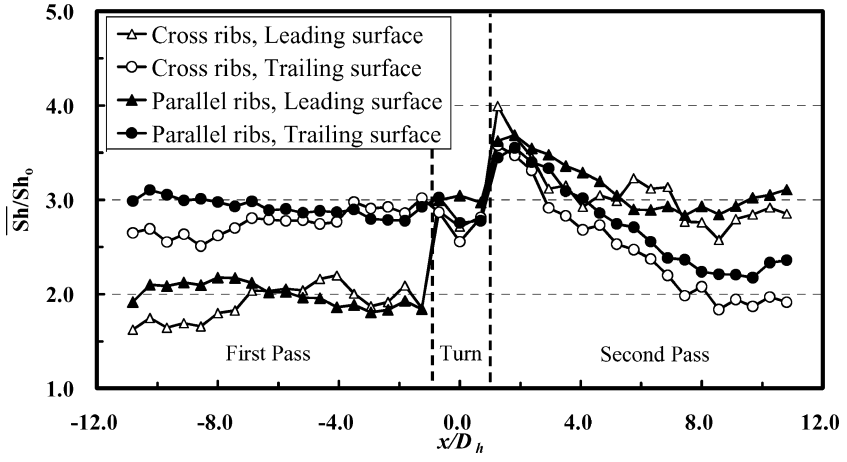

c) $Ro = 0.20$

Fig. 12 Comparison of regional averaged Sherwood number ratios.

same for most of the data points in the cross and parallel ribbed passages. When it is considered that the locations are in accordance with the impingement region of the turn-induced vortices, the comparison leads to the important conclusion that the effect of rotation overwhelms the effect of ribs at a high rotation number, especially from the entrance of the 180-deg turn to the upstream region of the second pass.

Figure 12 is the comparison of the regional averaged Sherwood number ratios for the cross and parallel rib arrangements. For the stationary cases shown in Fig. 12a, the ratios of leading and trailing surfaces in the parallel rib arrangement are higher than those of the cross rib arrangement. The secondary flow is stronger in the parallel case, thus, resulting in the higher heat/mass transfer. As the rotation number increases (Figs. 12b and 12c), the heat/mass transfer discrepancy between the leading and the trailing surfaces becomes larger. The effect of rotation overwhelms the effect of rib arrangements at the higher rotation numbers as shown in Fig. 12c. Therefore, almost the same Sherwood number ratios are obtained regardless of the rib arrangements, especially near the turning region, $-3.0 \leq x/D_h \leq 3.0$.

In the present study, comparisons with the calculated heat transfer values were not presented. It is known that computational fluid dynamics does not predict accurately the heat transfer values in complex separation and reattachment flows that take place between

successive ribs.[6] However, the calculated flow patterns were very suitable for explanations of the experimental heat transfer distributions.

Conclusions

Mass transfer experiments were conducted to comprehend the internal heat/mass transfer characteristics in a rotating ribbed passage with a 180-deg turn and the overall flow patterns in the passage were predicted to help in understanding heat transfer characteristics. The observations of the internal passage phenomena led to the following conclusions.

1) For the stationary case, rib turbulators induce a secondary flow cell in the first pass of the passage. The rib angle of attack determines mainly the rotating direction of the flow cell. One pair of vortices is produced in the parallel rib arrangement due to the geometrical symmetry of duct, whereas only one cell of secondary vortex is induced in the cross rib arrangement. The impingement effect of the rib-induced flow is greater in the parallel rib arrangement so that the regional averaged Sherwood number ratios in the first pass are approximately 2.9 times higher than those of the smooth passage, whereas they are only 2.5 times those for the cross ribbed case. For the turning region of the cross ribbed channel, the asymmetric rib-induced flow generates a large vortex cell close to the trailing surface, which induces the heat/mass transfer discrepancy in the second pass. The turn-induced vortex becomes weaker, mixing with the rib-induced secondary flow, near the outlet of the passage. As a result, the averaged Sherwood number ratios on the leading and trailing surfaces approach each other again.

2) For the rotating cases, the flowfields in the first pass reveal that velocity vectors move to the trailing surface, and thus, heat/mass transfer on the corresponding wall is enhanced. On the 90-deg plane of the turn, the deflected main flow from the first pass enlarges the vortex cell close to the leading surface, and the small vortex cell on the trailing surface side contracts to disappear as the passage channel rotates faster. The prediction of those flow structures explains the change of heat/mass transfer behavior in the upstream region of the second pass. The rotation effect changes the heat/mass transfer behavior, especially in the turning region and the upstream region of the second pass. The heat/mass transfer discrepancy is observed from the comparisons of regional averaged Sherwood number ratios.

3) The overall flow structure in the second pass is similar to that of the smooth passage. Particularly at the highest tested rotation number, $Ro = 0.20$, the turn-induced single vortex cell affects dominantly the flow and heat/mass transfer characteristics around the 180-deg turn regardless of the rib configuration. Therefore, the effect of rib turbulators becomes less significant and similar heat/mass transfer distributions are observed for all of the test sections.

Acknowledgment

This research was supported by Korean Ministry of Science and Technology through its National Research Laboratory program.

References

[1]Han, J. C., Park, J. S., and Lei, C. K., "Heat Transfer Enhancement in Channels With Turbulence Promoters," *Journal of Engineering for Gas Turbines and Power*, Vol. 107, No. 3, 1985, pp. 628–635.

[2]Olsson, C.-O., and Sunden, B., "Experimental Study of Flow and Heat Transfer in Rib-roughened Rectangular Channels," *Experimental Thermal and Fluid Science*, Vol. 16, No. 4, 1998, pp. 349–365.

[3]Chen, Y., Nikitopoulos, D. E., Hibbs, R., Acharya, S., and Myrum, T. A., "Detailed Mass Transfer Distribution in a Ribbed Coolant Passage With a 180° Bend," *International Journal of Heat and Mass Transfer*, Vol. 43, No. 8, 2000, pp. 1479–1492.

[4]Iacovides, H., and Raisee, M., "Recent Progress in the Computation of Flow and Heat Transfer in Internal Cooling Passages of Turbine Blades," *International Journal of Heat and Fluid Flow*, Vol. 20, No. 3, 1999, pp. 320–328.

[5]Miyake, Y., Tsujimoto, K., and Nakaji, M., "Direct Numerical Simulation of Rough-wall Heat Transfer in a Turbulent Channel Flow," *International Journal of Heat and Fluid Flow*, Vol. 22, No. 3, 2001, pp. 237–244.

[6]Ooi, A., Iaccarino, G., Durbin, P. A., and Behnia, M., "Reynolds Averaged Simulation of Flow and Heat Transfer in Ribbed Ducts," *International Journal of Heat and Fluid Flow*, Vol. 23, No. 6, 2002, pp. 750–757.

[7]Bonhoff, B., Parneix, S., Leusch, J., Johnson, B. V., Schabacker, J., and Bölcs, A., "Experimental and Numerical Study of Developed Flow and Heat Transfer in Coolant Channels With 45 Degree Ribs," *International Journal of Heat and Fluid Flow*, Vol. 20, No. 3, 1999, pp. 311–319.

[8]Murata, A., and Mochizuki, S., "Comparison Between Laminar and Turbulent Heat Transfer in a Stationary Square Duct with Transverse or Angled Rib Turbulators," *International Journal of Heat and Mass Transfer*, Vol. 44, No. 6, 2001, pp. 1127–1141.

[9]Taslim, M. E., Bondi, L. A., and Kercher, D. M., "An Experimental Investigation of Heat Transfer in an Orthogonally Rotating Channel Roughened With 45 deg Criss-Cross Ribs on Two Opposite Walls," *Journal of Turbomachinery*, Vol. 113, No. 3, 1991, pp. 346–353.

[10]Al-Qahtani, M., Chen, H.-C., and Han, J.-C., "A Numerical Study of Flow and Heat Transfer in Rotating Rectangular Channels (AR = 4) With 45° Rib Turbulators by Reynolds Stress Turbulence Model," American Society of Mechanical Engineers, ASME Paper GT-2002-30216, June 2002.

[11]Park, C. W., Lau, S. C., and Kukreja, R. T., "Heat/Mass Transfer in a Rotating Two-Pass Channel With Transverse Ribs," *Journal of Thermophysics and Heat Transfer*, Vol. 12, No. 1, 1998, pp. 80–86.

[12]Park, C. W., Lau, S. C., and Kukreja, R. T., "Heat (Mass) Transfer in a Rotating Channel with Ribs of Various Sizes on Two Walls," *Journal of Thermophysics and Heat Transfer*, Vol. 12, No. 3, 1998, pp. 452–454.

[13]Lin, Y.-L., Shih, T. I.-P., Stephens, M. A., and Chyu, M. K., "A Numerical Study of Flow and Heat Transfer in a Smooth and Ribbed U-Duct With and Without Rotation," *Journal of Heat Transfer*, Vol. 123, No. 2, 2001, pp. 219–232.

[14]Hwang, G. J., Tzeng, S. C., Mao, C. P., and Soong, C. Y., "Heat Transfer in a Radially Rotating Four-Pass Serpentine Channel With Staggered Half-V Rib Turbulators," *Journal of Heat Transfer*, Vol. 123, No. 1, 2001, pp. 39–50.

[15]Lee, E., Wright, L. M., and Han, J. C., "Heat Transfer in Rotating Rectangular Channels with V-Shaped and Angled Ribs," *Journal of Thermophysics and Heat Transfer*, Vol. 19, No. 1, 2005, pp. 48–56.

[16]Liou, T.-M., Chen, M.-Y., and Wang, Y.-M., "Heat Transfer, Fluid Low and Pressure Measurements Inside a Rotating Two-Pass Duct With Detached 90° Ribs," American Society of Mechanical Engineers, ASME Paper GT2002-30201, June 2002.

[17]Cho, H. H., Wu, S. J., and Kim, W. S., "A Study on Heat Transfer Characteristics in a Rib-roughened Rectangular Duct," *Proceedings of 11th International Symposium on Transport Phenomena*, Pacific Center of Thermal-Fluids Engineering, HI, 1998, pp. 364–369.

[18]Cho, H. H., Wu, S. J., and Kwon, H. J., "Local Heat/Mass Transfer Measurements in a Rectangular Duct With Discrete Ribs," *Journal of Turbomachinery*, Vol. 122, No. 3, 2000, pp. 579–586.

[19]Cho, H. H., Lee, S. Y., Wu, S. J., "The Combined Effects of Rib Arrangements and Discrete Ribs on Local Heat/Mass Transfer in a Square Duct," American Society of Mechanical Engineers, ASME Paper 2001-GT-175, June 2001.

[20]Cho, H. H., Kim, Y. Y., Rhee, D. H., Lee, S. Y., Wu, S. J., and Choi, C., "The Effects of Gap Position in Discrete Ribs on Local Heat/Mass Transfer in a Square Duct," *Journal of Enhanced Heat Transfer*, Vol. 10, No. 3, 2002, pp. 287–300.

[21]Cho, H. H., Lee, S. Y., Rhee, D. H., and Won, J. H., "Heat Transfer Characteristics in a Two-Pass Rotating Rectangular Duct with 70° Attack Angle Ribs," *Proceedings of the International Conference on Energy Conversion and Application*, Huazhong Univ. Science and Technology Press, Wuhan, PRC, 2001, pp. 605–610.

[22]Cho, H. H., Lee, S. Y., Rhee, D. H., Joo, W. G., and Lee, J. H., "Effects of Rib Configurations on Heat/Mass Transfer In a Two-Pass Rotating Duct," 9th International Symposium on Transport Phenomena and Dynamics of Rotating Machinery, Paper HT-ABS-024, Pacific Center of Thermal-Fluids Engineering, HI, June 2002.

[23]Cho, H. H., Lee, S. Y., and Rhee, D. H., "Effects of Cross Ribs on Heat/Mass Transfer in a Two-Pass Rotating Duct," *Heat and Mass Transfer*, Vol. 40, No. 10, 2004, pp. 743–755.

[24]Kim, K. M., Kim, Y. Y., Rhee, D. H., and Cho, H. H., "An Investigation of Duct Aspect Ratio Effects on Heat/Mass Transfer in a Rotating Duct with 90° Ribs," American Society of Mechanical Engineers, ASME Paper GT2004-53533, June 2004.

[25]Kim, K. M., Kim, Y. Y., Rhee, D. H., and Cho, H. H., "Local Heat/Mass Transfer Phenomena in Rotating Passage, Part 1: Smooth Passage," *Journal of Thermophysics and Heat Transfer*, Vol. 20, No. 2, 2006, pp. 188–198.

[26]Kline, S. J., and McClintock, F. A., "Describing Uncertainty in Single-sample Experiments," *Mechanical Engineering*, Vol. 75, Jan. 1953, pp. 3–8.

[27]McAdams, W. H., *Heat Transmission*, 2nd ed. McGraw–Hill, New York, 1942, Chap. 9.

[28]"Fluent 6.1 User's Guide," Vol. 2, Fluent, Inc., Lebanon, NH, 2003, Chap. 8–19.